Available online at www.sciencedirect.com
ScienceDirect
Catalysis Today 137 (2008) 253–260
CATALYSIS TODAY
www.elsevier.com/locate/cattod

Dynamics and selectivity of NO_x reduction in NO_x storage catalytic monolith

Petr Kočí [a,c,*], František Plát [a,c], Jan Štěpánek [a,c], Milan Kubíček [b,c], Miloš Marek [a,c]

[a] Department of Chemical Engineering, Institute of Chemical Technology, Prague, Technická 5, CZ-166 28 Praha, Czech Republic
[b] Department of Mathematics, Institute of Chemical Technology, Prague, Technická 5, CZ-166 28 Praha, Czech Republic
[c] Center for Nonlinear Dynamics of Chemical and Biological Systems, Institute of Chemical Technology, Prague, Technická 5, CZ-166 28 Praha, Czech Republic

Available online 3 January 2008

Abstract

Several nitrogen compounds can be produced during the regeneration phase in periodically operated NO_x storage and reduction catalyst (NSRC) for conversion of automobile exhaust gases. Besides the main product N_2, also NO, N_2O, and NH_3 can be formed, depending on the regeneration phase length, temperature, and gas composition. This contribution focuses on experimental evaluation of the NO_x reduction dynamics and selectivity towards the main products (NO, N_2 and NH_3) within the short rich phase, and consequent development of the corresponding global reaction-kinetic model. An industrial NSRC monolith sample of PtRh/Ba/CeO_2/ γ-Al_2O_3 type is employed in nearly isothermal laboratory micro-reactor. The oxygen and NO_x storage/reduction experiments are performed in the temperature range 100–500 °C in the presence of CO_2 and H_2O, using H_2, CO and C_3H_6 as the reducing agents.

The spatially distributed NSRC model developed earlier is extended by the following reactions: NH_3 is formed by the reaction of H_2 with NO_x and it can further react with oxygen and NO_x deposited on the catalyst surface, producing N_2. Considering this scheme with ammonia as an active intermediate of the NO_x reduction, a good agreement with experiments is obtained in terms of the NO_x reduction dynamics and selectivity. A reduction front travelling in the flow direction along the reactor is predicted, with the NH_3 maximum on the moving boundary. When the front reaches the reactor outlet, the NH_3 peak is observed in the exhaust gas. It is assumed that the ammonia formation during the NO_x reduction by CO and HCs at higher temperatures proceed via the water gas shift and steam reforming reactions producing hydrogen. It is further demonstrated that oxygen storage effects influence the dynamics of the stored NO_x reduction. The temperature dependences of the outlet ammonia peak delay and the selectivity towards NH_3 are correlated with the effective oxygen and NO_x storage capacity.

Keywords: NO_x storage catalyst; NO_x reduction selectivity; Exhaust gas conversion; Monolith; Mathematical modelling

1. Introduction

From the reaction-kinetic modelling point of view, the monolith washcoated by the NO_x storage and reduction catalyst (NSRC) [1] is one of the most complex automobile exhaust gas converters. Variety of different physical and chemical processes and the number of gas and surface components participating in typical periodic lean/rich operation form a large and closely linked system [2–7].

Primary application of the NSR catalyst is the elimination of the NO_x emissions from diesel and lean-burn gasoline engines, where direct NO_x reduction is hindered due to an excess of oxygen in the exhaust gas. In the course of a longer lean phase (economical engine operation with lean fuel mixture, typically lasting for several minutes) the NO_x are adsorbed (stored) on the catalyst surface in the form of nitrites and nitrates. Several NO_x adsorbing components (Ba, K, Na, Ca, Li, Mg, etc.) can be used simultaneously in the NSRC washcoat, with particular temperature dependence of the effective NO_x storage capacity related to the basicity of the used components [8]. Then, the accumulated NO_x are desorbed and reduced within a short rich

Abbreviations: GHSV, gas hourly space velocity (h^{-1}); HC, hydrocarbons; NM, noble metals; NSRC, NO_x storage and reduction catalyst.

* Corresponding author at: Department of Chemical Engineering, Institute of Chemical Technology, Prague, Technická 5, CZ-166 28 Praha, Czech Republic. Tel.: +420 22044 3293; fax: +420 22044 4320.
E-mail addresses: petr.koci@vscht.cz (P. Kočí), milos.marek@vscht.cz (M. Marek).
URL: http://www.vscht.cz/monolith

0920-5861/$ – see front matter © 2007 Elsevier B.V. All rights reserved.
doi:10.1016/j.cattod.2007.11.023

Nomenclature

k	reaction rate constant, dimension depends on the reaction
K_a	inhibition constant
K_y^{eq}	thermodynamic equilibrium constant, 1
R	reaction rate (mol m^{-3} s^{-1}) (related to washcoat volume)
S	reaction selectivity, 1
t	time (s)
T	gas temperature (K)
y	mole fraction of gas component, 1
z	spatial coordinate along the monolith reactor (m)

Greek letters

τ	time interval (s)
ψ	coverage of the surface-deposited component, 1
ψ^{eq}	temperature-dependent saturation (equilibrium) coverage, 1
Ψ^{cap}	absolute storage capacity (mol m^{-3}) (related to washcoat volume)

Subscripts and superscripts

eq	equilibrium
exp	experiment
in	inlet
j	index of reaction
k	index of gas component
m	index of surface-deposited component
out	outlet
red	reduction
reg	regeneration
sim	simulation

phase (excess of reducing components CO, H_2 and HCs in the exhaust gas, lasting several seconds). The exhaust gas enrichment can be realised by controlled (post-)injection of rich fuel mixture or other techniques that result in temporary excess of reducing components in the exhaust gas [9].

Different adsorption mechanisms take part simultaneously during the NO_x storage [2]. The storage process is influenced by the NO oxidation to NO_2 and by the transformation of different forms of the stored NO_x(nitrite and nitrate route) [10–12]. A competitive adsorption of other gases present in the exhaust gas (namely CO_2, H_2O, and SO_2) occurs on the NO_x storage sites [13,14] which has to be taken into account in the real exhaust gas system. The NO_x storage rate is also inherently influenced by internal diffusion effects [15–17] and by the proximity of the NO_x storage material and noble metal sites [18].

It is well-known that several nitrogen compounds may be produced during the regeneration phase, depending on the gas temperature, composition (red/ox ratio, reduction by H_2, CO and HCs) and the length of the regeneration phase—NO, N_2O, N_2, and NH_3, cf., e.g. [5,6,19]. The processes within the short rich phase are highly transient, involving internal transport effects, interactions between NO_x storage components, catalytic noble metals and oxygen storage materials [2,3,6,20]. Heat evolution effects also play an important role under nearly adiabatic conditions in real monolith reactor [21]. The molecular nitrogen is usually the main and desired product of the NO_x reduction. The NO peak at the beginning of the regeneration phase results from the sudden desorption of the stored NO_x without efficient reduction. Smaller amounts of N_2O are formed mostly below and around the light-off temperature of the used reducing agent as the product of the incomplete NO_x reduction [2,5,6]. During the rich phase, the reducing front is travelling along the channel from the inlet to the outlet [2,3,5,20]. The main ammonia outlet peak then appears after several seconds, when the catalyst surface along the monolith channel is reduced and an excess of the reducing agents occurs at the monolith outlet. Recently it has been proposed, that the ammonia produced at the front part of the monolith can react with the NO_x deposited on the unreduced catalyst surface at the rear part of the monolith, producing mainly N_2 [5,7]. It was also proved experimentally that ammonia is an active intermediate in the regeneration of NSRC with H_2 [7]: when NH_3 was used directly at the reactor inlet instead of H_2, the NO_x reduction process was equivalent to the regeneration by H_2.

In this contribution we focus on experimental evaluation of the NO_x reduction dynamics and selectivity towards the main products (NO, N_2 and NH_3) during the NSRC regeneration by H_2, CO and C_3H_6 in the presence of CO_2 and H_2O, and the consequent development of effective global reaction-kinetic model that is able to describe the observed phenomena. Particularly, we pay attention to the observed correlation of NH_3 breakthrough time and the effective NO_x and O_2 storage capacity. The spatially distributed NSRC monolith model with global kinetics developed earlier [3] is extended by the ammonia formation and decomposition reactions and the simulation results are compared with the measurements.

2. Experiments

2.1. Experimental set-up

Lean/rich experiments have been carried out in nearly isothermal, modular steel micro-reactor, containing three (identical) small NSRC monolith samples in series [22]. The studied catalyst was an industrial PtRh/Ba/CeO_2/ γ-Al_2O_3 washcoated on 400 cpsi cordierite monolith. The size of each sample was 3 cm (width) $\times$ 2.5 cm (length) $\times$ 0.5 cm (height). Pre-treatment of the fresh catalyst samples was 1 h on stream at 500 °C with lean (oxidising) conditions and then 1 h lean/rich operation at 300 °C (cf. Table 1). No change of catalyst activity or storage capacity was then observed in the course of experimental series. Before each experiment, the stored NO_x were removed from the catalyst surface by the reduction using rich mixture of H_2 + O_2 at 400 °C (cf. Table 1).

Temperature was measured in front of and behind each sample. Inlet gas temperature in the course of each experiment was constant. The reaction mixture was prepared on-line from synthetic gases, representing basic components in automobile

Table 1
Conditions in the lean (storage) and rich (regeneration) phase used in experiments and simulations

Variable	Lean phase (storage)	Rich phase (regeneration)
τ	300 s	20 s
GHSV	30,000 h^{-1}	30,000 h^{-1}
T^{in}	100–500 °C	100–500 °C
y^{in}_{NO}	500 ppm [a]	500 ppm [a]
$y^{in}_{NO_2}$	0 ppm	0 ppm
$y^{in}_{O_2}$	7%	0.2%
$y^{in}_{H_2}$	0%	3.3% [b]
y^{in}_{CO}	0%	3.3% [b]
$y^{in}_{C_3H_6}$	0 ppm	3667 ppm [b]
$y^{in}_{NH_3}$	0 ppm	0 ppm
$y^{in}_{CO_2}$	5%	5%
$y^{in}_{H_2O}$	5%	5%
$y^{in}_{N_2}$	Balance	Balance

Inlet gas composition is given in mol. fractions.
[a] In the case of oxygen storage and reduction experiments, the inlet NO_x concentration is zero.
[b] Just one reducing agent (either H_2, or CO, or C_3H_6) was used in each experiment. The propene concentration is equivalent to those of CO and H_2 with respect to the redox reactions stoichiometry.

exhaust gas: CO, O_2, C_3H_6, H_2, NO, CO_2 and H_2O, which were admixed to N_2 (carrier gas). Concentrations of the individual components were continuously set by fast mass-flow controllers with response time to the lean/rich step change approximately 1 s. The flow-rate was GHSV = 30,000 h^{-1} and the inlet gas always contained 5% H_2O and 5% CO_2. The conditions used in the experiments and simulations are summarised in Table 1. On-line IR absorption analysers (ABB Advanced Optima Uras) were employed for CO and CO_2 measurements in the outlet gas. The concentrations of nitrogen compounds NO, NO_2 and NH_3 were detected by UV absorption analysers (ABB Advanced Optima Limas). The O_2, HC and H_2 concentrations were analysed by mass spectrometer (Pfeiffer Vacuum Omnistar GSD301). The sampling lines were heated to 180 °C to minimise the adsorption or condensation of the gas components, and to prevent the formation of solid compounds.

2.2. Experimental results

Dynamic behaviour of the NSRC samples was studied during periodic lean/rich (300/20 s) operation at temperatures 100, 150, 200, 250, 300, 350, 400, 450 and 500 °C. All three reducing agents (H_2, CO and C_3H_6) were examined individually. Stoichiometry-equivalent concentration levels of the reducing agents were used (cf. Table 1, all three rich mixtures provide the same red/ox ratio) in order to enable direct comparison of their NO_x reduction activity. Examples of the measured evolution of the NO_x concentrations at two different temperatures are depicted in Fig. 1. At the lower temperature (Fig. 1a) the activity of the reducing agents in NO_x reduction decreases in the order $H_2 < CO < C_3H_6$, hence different reaction rates have to be considered for NO_x reduction by H_2, CO and C_3H_6 [3]. At the higher temperature (Fig. 1b) the NO_x

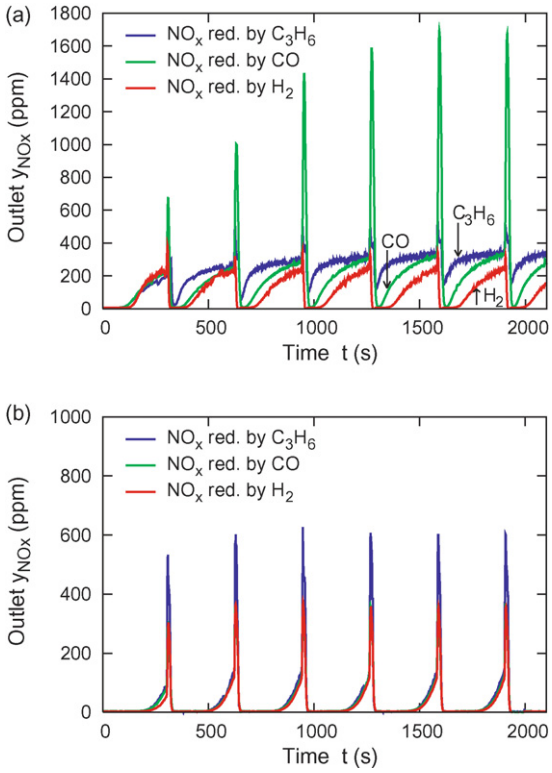

Fig. 1. Experimentally observed evolution of the outlet NO_x concentrations during periodic lean/rich operation (300/20 s)—comparison of the NO_x reducing agents (H_2, CO, and C_3H_6) at T^{in}=200 °C (a) and T^{in}=350 °C (b). Inlet concentrations are given in Table 1.

reduction efficiency is almost the same for all three reducing agents, which can be explained either by mass-transfer limited operation and/or by the transformation of CO and C_3H_6 to H_2 via the water gas shift and steam reforming reactions [3,4]. At the lower temperature (Fig. 1a) we can observe the effect of gradual stabilisation of the periodic operation in the case of incomplete reduction of the stored NO_x with CO and C_3H_6 [3,20].

The detail of the dynamic evolution of NO_x and NH_3 concentrations at the reactor outlet during the regeneration phase is given in Fig. 2 a. First the NO desorption peak is observed, and then the main ammonia peak appears at the later part of the regeneration. Concurrently with the increase of the NH_3 concentration, the NO concentration gradually decrease to zero. This sequence is quite general and holds for all three reducing agents in the studied temperature range, but with varying NH_3 breakthrough time, different NO and NH_3 peaks maxima and wider or narrower overlaps between the outlet NO and NH_3 peaks.

The outlet ammonia peaks observed at different temperatures with H_2 as the reducing agent are compared in Fig. 2 b. For the given lean/rich timing, the largest NH_3 peaks are emitted at lower temperatures (100–200 °C). The NH_3 breakthrough time increases with the increasing temperature and reaches maximum at 350 °C. Then, at high temperatures (400–500 °C), the ammonia breakthrough time decreases again, but the maxima of the peaks are relatively low. The breakthrough time of the reducing agent was found to be

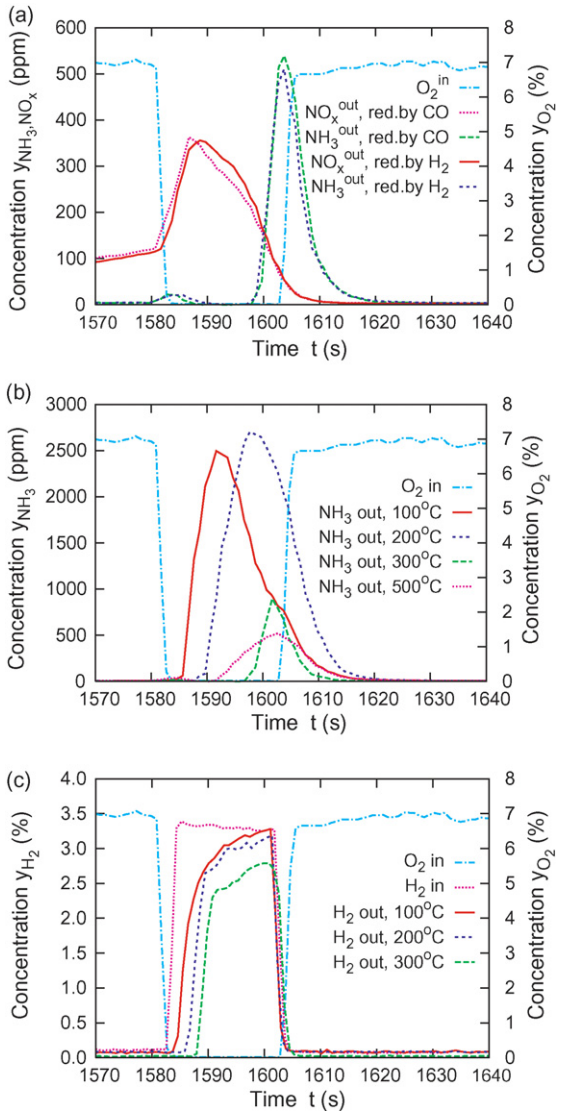

Fig. 2. Observed dynamics of the redox processes during the rich phase. The timing and the inlet concentrations are given in Table 1. (a) Standard lean/rich operation, NO_x + oxygen storage and reduction, T^{in}=350 °C, comparison of H_2 and CO as the reducing agent. (b) Standard lean/rich operation, NO_x + oxygen storage and reduction, H_2 as the reducing agent, comparison of different temperatures; the outlet H_2 breakthrough (not shown here) is synchronised with the NH_3 breakthrough at all studied temperatures. (c) Lean/rich operation without NO_x, only oxygen storage and reduction, H_2 as the reducing agent, comparison of different temperatures.

synchronised with the main NH_3 peak at all studied temperatures.

Not only the stored NO_x but also the oxygen deposited on the catalyst surface is involved in the redox processes during the regeneration phase. The results of the lean/rich operation without NO_x are shown in Fig. 2 c. In this case the amount of the consumed reducing agent is directly proportional to the effective oxygen storage capacity. Higher oxygen storage capacity then results in a longer delay of the reducing agent breakthrough.

If we assume the N_2 and NH_3 as the only products of the NO_x reduction, then the integral selectivity of the NO_x reduction towards NH_3 over stabilised periodic lean/rich operation with a constant flow-rate can be calculated from the following formula:

$$S_{NH_3} = \frac{\int_{t_1}^{t_2} y_{NH_3}^{out}\,dt}{(1/2)\int_{t_1}^{t_2}(y_{NO_x}^{in} - y_{NO_x}^{out} - y_{NH_3}^{out})\,dt} \quad (1)$$

Here t_1 and t_2 correspond to the beginning and the end of a stabilised lean + rich period, respectively. The S_{NH_3} value thus represents the overall NO_x reduction products ratio NH_3:N_2. The calculated temperature dependences of the S_{NH_3} for the individual reducing agents (H_2, CO and C_3H_6) are summarised in Fig. 3. It can be seen that the highest integral NH_3 selectivity is met at low temperature, but above the light-off temperature for the used reducing agent; the order of the light-off temperatures is H_2 ¡ CO ¡ C_3H_6 (cf. Fig. 1 a and [3,23]). For very low temperatures (¡200 °C) no ammonia formation is observed with CO and C_3H_6 as the reducing agents. On the other hand, the highest NH_3 selectivity is reached with hydrogen at the temperature 100 °C[1]. From these results it follows that hydrogen is the main active component responsible for the NH_3 formation. At higher temperatures (above 350 °C) the NH_3 selectivity is similar for all the reducing agents (cf. Fig. 2a), thus it is likely that the other reducing agents (CO and C_3H_6) produce NH_3 mostly via their transformation to hydrogen that takes place at higher temperatures (water gas shift and steam reforming) [3,4].

After looking at Fig. 3 and examining the temperature dependences of (i) the integral selectivity of the NO_x reduction towards NH_3 with the H_2 as the reducing agent (S_{NH_3}, H_2), (ii) the effective NO_x storage capacity ($\Psi_{NO_x}^{cap}.\psi_{NO_x}^{eq}$), and (iii) the effective oxygen storage capacity ($\Psi_{O_2}^{cap}.\psi_{O_2}^{eq}$), one may realise that these three curves are correlated in the following way: The integral NH_3 selectivity decreases with the increasing effective NO_x and oxygen storage capacity. This observation is consistent with the assumption that the main outlet NH_3 peak appears when the complete reduction of the catalyst surface is reached and the excess of reducing components occurs at the reactor outlet [5,7]. Thus, the higher effective NO_x and oxygen storage capacity of the catalyst result in a higher consumption of the reducing agent and a longer time till the NH_3 breakthrough, so that a lower integral NH_3 selectivity is reached for the constant lean/rich timing.

3. Mathematical modelling

In this section, a mathematical model is developed and employed for the solution of the reaction and transport processes inside the NSRC monolith. The aim of the model is to describe and predict the NO_x reduction dynamics and selectivity in the NSRC converter with minimum set of reactions and kinetic parameters that need to be evaluated from

[1] The highest amount of the emitted NH_3 is observed during the experiments at the temperature 150–200 °C, not the 100 °C. Note that the S_{NH_3} is just the ratio of the NO_x reduction products (NH_3:N_2), thus the absolute amount of the emitted NH_3 is not determined solely by the S_{NH_3} but also by the integral NO_x conversion, which is rather low at the lowest temperatures.

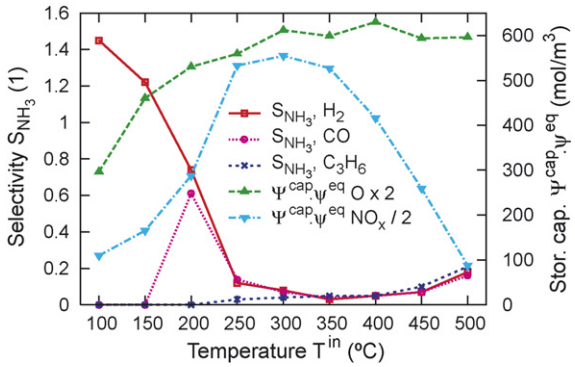

Fig. 3. Temperature dependences of the NO_x and oxygen storage capacity, and integral selectivity of the NO_x reduction towards NH_3 for periodic lean/rich operation (300/20 s) with H_2, CO or C_3H_6 as the reducing agent. Inlet concentrations are given in Table 1.

experimental data, while keeping the essential level of reliability.

3.1. Model of catalytic monolith

Spatially pseudo-1D, heterogeneous model of monolith channel with plug-flow and surface deposition of gas components is employed in the simulations [3,24]. Within this model, possible internal diffusion effects are lumped into effective reaction rate parameters for given washcoat structure. The following balances are considered: (i) component mass balances in the flowing gas, including accumulation, convection, and external mass transfer; (ii) component mass balances in the washcoat pores, including accumulation, external mass transfer, and catalytic reactions; (iii) mass balances of the components deposited on the catalyst surface, including accumulation, adsorption/desorption and catalytic reactions; (iv) enthalpy balance of the flowing gas, including accumulation, convection, and gas–solid heat transfer; and (v) enthalpy balance of the solid phase, including accumulation, axial heat conduction, gas–solid heat transfer, and heat source from catalytic reactions.

The finite differences method with semi-implicit approximations of time derivatives, first-order Taylor's expansion of reaction rates, and adaptive time-step control has been used to solve the model. The model has been implemented in Fortran into the versatile software package for dynamic simulations of interconnected systems of reactors and adsorbers, developed at the Institute of Chemical Technology, Prague [3,20,22,25–30].

3.2. Reaction modelling

The objective of global reaction model development is to construct the minimum set of reactions and kinetic parameters that need to be evaluated from experimental data, while keeping the adequate level of details to describe the experimentally observed phenomena. In this paper we focus on the dynamics and selectivity of the NO_x reduction in the NSRC monolith towards NH_3. The basic set of model reactions for NO_x storage and consequent reduction by H_2 is given in Table 2. The reaction scheme is derived from the spatially distributed NSRC model developed earlier [3], where N_2 was considered as the only product of the NO_x reduction. That reaction scheme has been modified and extended by the reactions involving NH_3 formation and decomposition.

In this extended model we consider that ammonia is formed by the reaction of H_2 with the NO_x from the inlet gas and the NO_x stored on the NSRC surface (r7 and r8 in Table 2). The formed NH_3 can further react with oxygen and NO_x, either coming from the inlet gas (r10 and r12), or deposited on the catalyst surface (r11 and r13). All the ammonia decomposition reactions are assumed to produce N_2 only (N_2O is not considered in this approximation). It is important to note that

Table 2
Model NSRC reactions with NH_3 as an active intermediate of the NO_x reduction by H_2

No.	Reaction	Model reaction rate
r1	$NO + \frac{1}{2}O_2 \rightleftharpoons NO_2$	$R_1 = k_1\left(y_{NO}\, y_{O_2}^{0.5} - \frac{y_{NO_2}}{K_{y,1}^{eq}}\right)\frac{1}{G_1}$
r2	$2NO_2 + BaCO_3 + \frac{1}{2}O_2 \rightarrow Ba(NO_3)_2 + CO_2$	$R_2 = k_2\, \Psi_{NO_x}^{cap}\, y_{NO_2}\, y_{O_2}^{0.1}(\psi_{NO_x}^{eq} - \psi_{NO_x})$
r3	$2\ NO + BaCO_3 + \frac{3}{2}O_2 \rightleftharpoons Ba(NO_3)_2 + CO_2$	$R_3 = k_3\, \Psi_{NO_x}^{cap}\, y_{NO}\, y_{O_2}^{0.1}(\psi_{NO_x}^{eq} - \psi_{NO_x})$
r4	$Ce_2O_3 + \frac{1}{2}O_2 \rightarrow Ce_2O_4$	$R_4 = k_4\, \Psi_{O_2}^{cap}\, y_{O_2}\left(\psi_{O_2}^{eq} - \psi_{O_2}\right)$
r5	$H_2 + Ce_2O_4 \rightarrow H_2O + Ce_2O_3$	$R_5 = k_5\, \Psi_{O_2}^{cap}\, y_{H_2}\, \psi_{O_2}$
r6	$H_2 + \frac{1}{2}O_2 \rightarrow H_2O$	$R_6 = k_6 y_{H_2}\, y_{O_2}\frac{1}{G_1}$
r7	$\frac{5}{2}H_2 + NO \rightarrow NH_3 + H_2O$	$R_7 = k_7\, y_{H_2}\, y_{NO}^{0.5}$
r8	$Ba(NO_3)_2 + 8H_2 \rightarrow 2NH_3 + 5H_2O + BaO$	$R_8 = k_8\, \Psi_{NO_x}^{cap} y_{H_2}\, \psi_{NO_x}\frac{1}{G_2}$
r9	$Ba(NO_3)_2 + 3H_2 \rightarrow 2NO + 3H_2O + BaO$	$R_9 = k_9\, \Psi_{NO_x}^{cap} y_{H_2}\, \psi_{NO_x}\frac{1}{G_3}$
r10	$2NH_3 + \frac{3}{2}O_2 \rightarrow N_2 + 3H_2O$	$R_{10} = k_{10} y_{NH_3}\, y_{O_2}$
r11	$2NH_3 + 3Ce_2O_4 \rightarrow N_2 + 3Ce_2O_3 + 3H_2O$	$R_{11} = k_{11}\, \Psi_{O_2}^{cap}\, y_{NH_3}\, \psi_{O_2}$
r12	$4NH_3 + 6NO \rightarrow 5N_2 + 6H_2O$	$R_{12} = k_{12}\, y_{NH_3}\, y_{NO}^{0.5}$
r13	$\frac{10}{3}NH_3 + Ba(NO_3)_2 \rightarrow \frac{16}{3}N_2 + 5H_2O + BaO$	$R_{13} = k_{13}\, \Psi_{NO_x}^{cap} y_{NH_3}\, \psi_{NO_x}\frac{1}{G_2}$
r14	$BaO + CO_2 \rightarrow BaCO_3$	$R_{14} = R_8 + R_9 + R_{13}$

$G_1 = (1 + K_{a,1}\, y_{CO} + K_{a,2}\, y_{C_3H_6})^2; \cdot (1 + K_{a,3}\, y_{CO}^2\, y_{C_3H_6}^2) \cdot (1 + K_{a,4}\, y_{NO_x}^{0.7})T$; $G_2 = 1 + K_{a,6}\, y_{O_2}$; $G_3 = (1 + 0.1\, K_{a,6}\, y_{O_2})(1 + K_{a,7}\, y_{NO_x})$. The form of the inhibition term G_1 is taken after [33]. The rate laws R_1– R_6, R_8, and R_{14} are taken from the global NSRC model without explicit consideration of NH_3 [3].

the stored components influence the redox balance during the rich reduction phase to a large extent. This reaction sequence is in agreement with our experimental data, as well as with the observations reported recently by other researchers studying the NSRC regeneration by H_2[5–7,19].

Two NO_x storage pathways are distinguished in the model (Table 2): the NO_2 adsorption and the slower NO adsorption via the nitrite route [11](the summary reactions r2 and r3, respectively). The reversible NO oxidation is described by the reaction r1. The oxygen storage and reduction effects, important for the balance of the reducing agent during the NSRC regeneration, are included in the form of reactions r4 and r5, respectively. Hydrogen oxidation by the spare oxygen in the rich phase has to be also counted in (cf. the reaction r6). In addition to the ''direct'' reduction of the NO_x stored on the Ba sites enabling spill-over to the noble metal sites (described by the summary reactions r8 and r13), the reducing-agent induced desorption of the stored NO_x in the form of NO is considered (r9). The desorbed NO can be then further reduced over noble metal sites (r7 and r12).

In the complete NSRC model with H_2, CO and C_3H_6 as the reducing agents, the following reactions are considered in addition with individual reaction rates and light-off temperatures (cf. [3]): CO and C_3H_6 oxidation, desorption and reduction of the stored NO_x by CO and C_3H_6, interaction of CO and C_3H_6 with the stored oxygen, and the water gas shift and steam reforming reactions. We assume that the ammonia formation observed during the NO_x reduction by CO and C_3H_6 in the presence of water at higher temperatures (cf. Fig. 3) can proceed via the water gas shift and steam reforming reactions, producing hydrogen. This assumption is supported by the measured light-off curves for these reactions (cf. [3])—the temperatures for the start of H_2 production from CO and C_3H_6 correspond approximately to those for the start of NH_3 formation (cf. the NH_3 selectivity curves for CO and C_3H_6 in Fig. 3). However, this hypothesis needs to be proved yet by the calculations with the complete NSRC model.

In the proposed global reaction-kinetic scheme (Table 2), a combination of pseudo-stationary kinetics and transient kinetics with the explicit consideration of the most important surface-deposited components (NO_x and O_2) is used. Several rate laws have been kept from the older models (cf. the footnote in Table 2). The storage phenomena are characterised by the maximum storage capacities Ψ_m^{cap}, temperature dependences of the relative saturation (equilibrium) coverages $\psi_m^{eq}(T)$ and global rate constants for the reaction processes $k_j(T)$. In comparison with more detailed NSRC micro-kinetic models (e.g. [31]), this approach gives a lower number of reaction steps and unknown kinetic parameters that need to be evaluated from experimental data. The resulting model then enables NSRC monolith simulations with the real exhaust gas in comfortable computation times, but with reasonable reliability and robustness [3,24,32]. The estimation of model kinetic parameters was done by adaptive simplex optimisation method, minimising the weighted sum of squares of differences between the experimental data and the model predictions.

3.3. Model results

Comparison of the simulation results with the experimental data is given in Fig. 4. The developed model describes correctly the slow NO_x adsorption during the lean phase, as well as the dynamics of the shorter rich phase, including the consequent evolution of the NO and NH_3 outlet peaks. The maxima of the peaks predicted by the model are higher and sharper than those observed in the experiments, however, it has to be considered that the measured concentrations are burdened by the signal dispersion occurring in the analysers. Total amount of the NO_x and NH_3 emitted during the peaks should be considered rather than the sharp peak maxima, and this criterion is matched quite well.

The corresponding evolution of spatially distributed concentration profiles inside the NSRC monolith reactor during the 20 s regeneration phase is depicted in Fig. 5a–f. Here the time t_{reg} is counted from the switch from the lean to the rich gas composition. At the end of the lean phase (Fig. 5a, t_{reg}=0 s), the catalyst surface is oxidised—the oxygen storage capacity is saturated uniformly, while the NO_x are stored mostly in the front part of the monolith, as the NO_x adsorption front proceeded from the reactor inlet to the outlet and the regeneration came before the complete NO_x breakthrough.

After 5 s of the regeneration (Fig. 5b), the front part of the monolith is already reduced, i.e., the NO_x and oxygen coverages are close to zero. A minor decrease of the hydrogen concentration can be observed just close to the monolith inlet. This decrease is caused by the H_2 reactions with the spare oxygen and NO (r6 and r7 in Table 2). The major H_2 consumption takes place on the boundary between the reduced

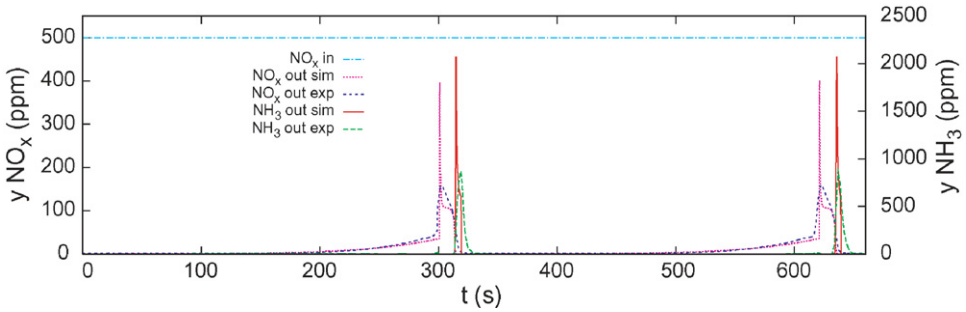

Fig. 4. Evolution of the outlet NO_x and NH_3 concentrations during periodic lean/rich operation (300/20 s)—comparison of experiment and model. Regeneration by H_2, T^{in}=300 °C, inlet concentrations are given in Table 1.

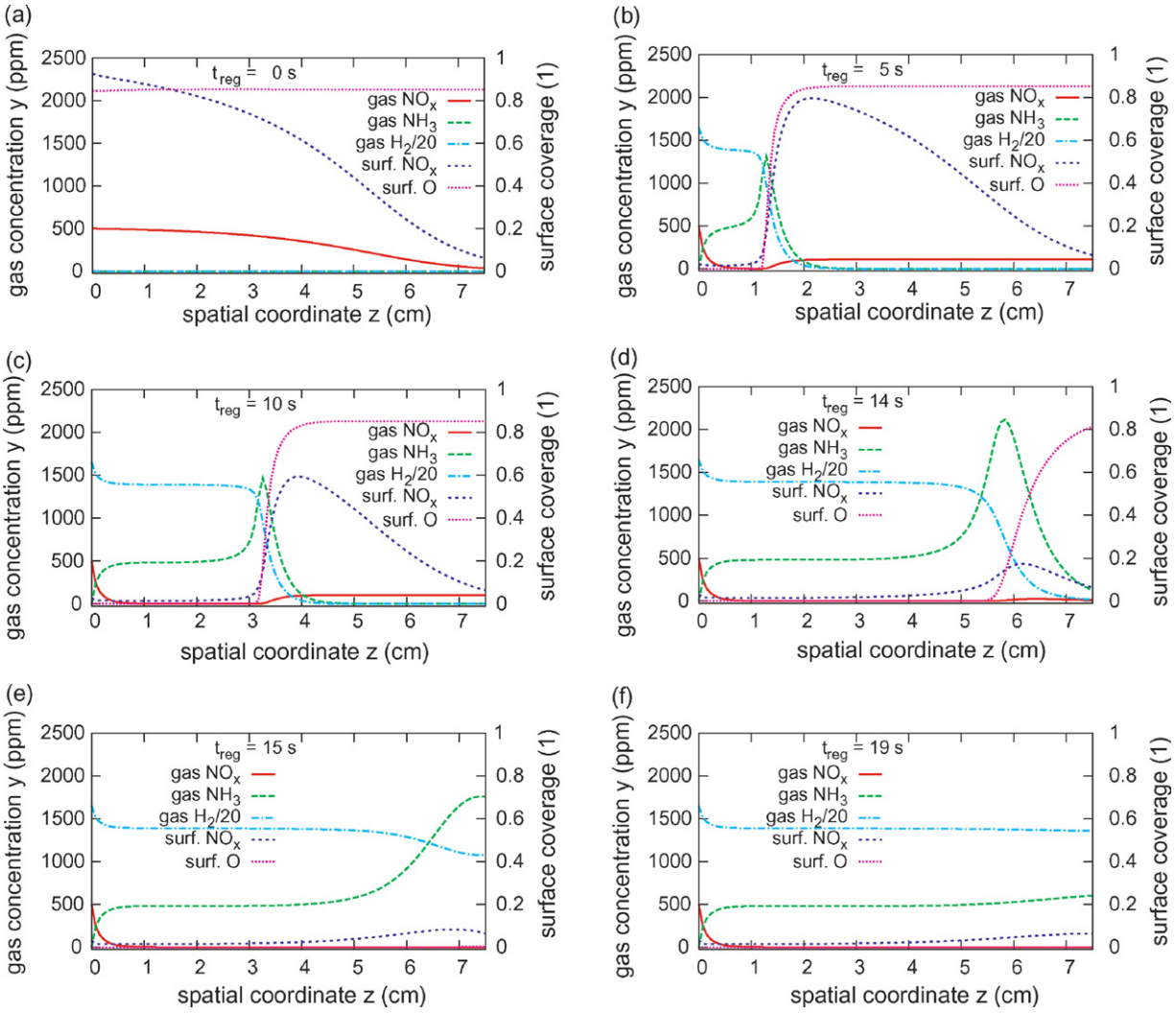

Fig. 5. Evolution of concentration profiles inside the reactor during the NSRC regeneration by H_2 (after 300 s of the NO_x storage) predicted by the model. Time of the regeneration t_{reg} is counted from the lean → rich switch. T^{in}=300 °C, inlet concentrations are given in Table 1. The position $z = 0$ cm corresponds to the reactor inlet, $z = 7.5$ cm corresponds to the reactor outlet.

(front) part and the non-reduced (rear) part of the monolith. Here the H_2 is employed in the reduction of the surface-deposited NO_x and oxygen (r5, r8 and r9) and its concentration drops to zero.

The gas-phase NO_x concentration decreases first to zero due to the NO_x reduction by H_2 (r7), but then it increases again on the redox boundary, because of the NO desorption from the stored NO_x (r9). The ammonia concentration increases from zero at the reactor inlet, first to the level corresponding to the reduction of gas-phase NO by H_2 (r7). Much higher increase is then caused by the reduction of the stored NO_x (r8) at the redox boundary. Behind the sharp maximum the NH_3 concentration decreases again, as the NH_3 is consumed by the reactions with the stored oxygen and NO_x (r11 and r13) in the rear, unreduced part of the monolith. In that moment, no NH_3 nor H_2 peak is observed yet at the monolith outlet.

From the following evolution of the concentration profiles in time it can be seen that the reduction front (represented by the redox boundary) is travelling along the monolith channel towards the reactor outlet. The speed of the front movement is not constant, it depends on the local coverage of the stored NO_x and oxygen. The higher initial NO_x coverage at the front part of the monolith results in a slower movement of the reduction front (higher amount of the reducing agents is consumed for the reduction of the catalyst surface), while the lower initial NO_x coverage speeds-up the reduction front in the rear part of the monolith—compare the position of the reduction front in Fig. 5a–c and (e) (in 5 s intervals). The redox front is also becoming more dispersed during the travelling along the monolith.

When the head of the redox front reaches the monolith outlet, the ammonia and reducing agent peaks appear in the outlet gas (cf. Figs. 4 and 5d and e). From the described mechanism of the NH_3 formation and decomposition distributed along the monolith it follows that the quantity of the NH_3 emitted into the outlet gas is influenced mainly by the local NO_x coverage at the rear part of the monolith. On the last profile near the end of the regeneration phase (Fig. 5f, t_{reg}=19 s) the

catalyst surface is almost completely reduced and prepared for the next lean (storage) phase.

4. Conclusions

The aim of the paper has been to study dynamics and selectivity of the NO_x reduction in an industrial type of NSRC monolith, and to develop an effective global reaction model that could be used for simulations of the real NSRC converter operation. The reaction scheme has been constructed with minimum set of reactions and kinetic parameters that need to be evaluated from experimental data, while keeping the essential level of model reliability. However, even with this ''simplified'' approach a relatively large effort is needed to cover the entire range of NSRC operating conditions, i.e., the temperatures 100–500 °C and the effects of individual reducing agents (H_2, CO and HC) on the periodic lean/rich operation. The basic set of ammonia formation and decomposition reactions has been proposed, considering NH_3 as an active intermediate of the NO_x reduction by H_2. These reactions include interaction of NH_3 with the oxygen and NO_x stored on the catalyst surface—the stored components influence the redox balance during the rich reduction phase to a large extent. The ammonia formation observed during the NO_x reduction by CO and C_3H_6 in the presence of water at higher temperatures is assumed to proceed via the water gas shift and steam reforming reactions, producing hydrogen. The experiments necessary for the evaluation of the model reaction parameters have been described and examples of the measured data have been given. The presented simulation results show that the proposed global kinetic model provides correct results with respect to the observed dynamics and selectivity of the NO_x reduction in NSRC monolith. The reduction front travelling along the monolith (predicted by the model) and the corresponding evolution of the outlet NO_x and NH_3 concentrations give a consistent insight into the spatially distributed redox processes inside the NSRC monolith during the regeneration phase.

Acknowledgements

The work was supported by the Czech Grant Agency (grant No. 104/05/2616) and the Czech Ministry of Education (project MSM 6046137306).

References

[1] N. Takahashi, H. Shinjoh, T. Iijima, T. Suzuki, K. Yamazaki, K. Yokota, H. Suzuki, N. Miyoshi, S. Matsumoto, T. Tanizawa, T. Tanaka, S. Tateishi, K. Kasahara, Catal. Today 27 (1996) 63.
[2] W.S. Epling, L.E. Campbell, A. Yezerets, N.W. Currier, J.E. Parks, Catal. Rev. 46 (2004) 163.
[3] P. Kočí, M. Schejbal, J. Trdlička, T. Gregor, M. Kubíček, M. Marek, Catal. Today 119 (2007) 64.
[4] J.-S. Choi, W.P. Partridge, W.S. Epling, N.W. Currier, T.M. Yonushonis, Catal. Today 114 (2006) 102.
[5] J.A. Pihl, J.E. Parks II, C.S. Daw, T.W. Root, SAE Tech. Paper 2006-01-3441, 2006.
[6] W.S. Epling, A. Yezerets, N.W. Currier, Appl. Catal. B: Environ. 74 (2007) 117.
[7] L. Cumaranatunge, S.S. Mulla, A. Yezerets, N.W. Currier, W.N. Delgass, F.H. Ribeiro, J. Catal. 246 (2007) 29.
[8] T. Kobayashi, T. Yamada, K. Kayano, SAE Tech. Paper 970745, 1997.
[9] http://www.dieselnet.com, 2007.
[10] I. Nova, L. Castoldi, L. Lietti, E. Tronconi, P. Forzatti, F. Prinetto, G. Ghiotti, J. Catal. 222 (2004) 377.
[11] I. Nova, L. Lietti, L. Castoldi, E. Tronconi, P. Forzatti, J. Catal. 239 (2006) 244.
[12] Y. Su, M.D. Amiridis, Catal. Today 96 (2004) 31.
[13] L. Lietti, P. Forzatti, I. Nova, E. Tronconi, J. Catal. 204 (2001) 175.
[14] H.Y. Huang, R.Q. Long, R.T. Yang, Appl. Catal. B 33 (2001) 127.
[15] J.S. Hepburn, E. Thanasiu, D.A. Dobson, W.L. Watkins, SAE Tech. Paper 962051, 1996.
[16] R.L. Muncrief, P. Khanna, K.S. Kabin, M.P. Harold, Catal. Today 98 (2004) 393.
[17] U. Tuttlies, V. Schmeißer, G. Eigenberger, Chem. Eng. Sci. 59 (2004) 4731.
[18] W.S. Epling, J.E. Parks, G.C. Campbell, A. Yezerets, N.W. Currier, L.E. Campbell, Catal. Today 96 (2004) 21.
[19] F. Basile, G. Fornasari, A. Gambatesa, M. Livi, A. Vaccari, Catal. Today 119 (2007) 59.
[20] P. Kočí, M. Kubíček, M. Marek, T. Maunula, M. Härkönen, Chem. Eng. J. 97 (2004) 131.
[21] S. Kojima, N. Baba, S. Matsunaga, K. Senda, K. Katoh, T. Itoh, SAE Technical Paper 2001-01-1297, 2001.
[22] http://www.vscht.cz/monolith, 2007.
[23] H. Abdulhamid, J. Dawody, E. Fridell, M. Skoglundh, J. Catal. 244 (2006) 169.
[24] A. Güthenke, D. Chatterjee, M. Weibel, B. Krutzsch, P. Kočí, M. Marek, I. Nova, E. Tronconi, Current status of modelling lean exhaust gas after treatment catalysts, in: G.B. Marin (Ed.), Advances in Chemical Engineering, vol. 33: Automotive Emission Control, Elsevier, 2008, pp. 103–211.
[25] J. Jirát, M. Kubíček, M. Marek, Catal. Today 53 (1999) 583.
[26] J. Jirát, M. Kubíček, M. Marek, Chem. Eng. Sci. 56 (2001) 1597.
[27] P. Kočí, M. Kubíček, M. Marek, Ind. Eng. Chem. Res. 43 (2004) 4503.
[28] D. Kryl, P. Kočí, M. Kubíček, M. Marek, T. Maunula, M. Härkönen, Ind. Eng. Chem. Res. 44 (2005) 9524.
[29] P. Kočí, F. Štěpánek, M. Kubíček, M. Marek, Chem. Eng. Sci. 61 (2006) 3240.
[30] P. Kočí, F. Štěpánek, M. Kubíček, M. Marek, Mol. Simul. 33 (2007) 369.
[31] L. Olsson, E. Fridell, M. Skoglundh, B. Andersson, Catal. Today 73 (2002) 263.
[32] A. Güthenke, D. Chatterjee, M. Weibel, N. Waldbüßer, P. Kočí, M. Marek, M. Kubíček, Chem. Eng. Sci. 62 (2007) 5357.
[33] S. Voltz, C. Morgan, D. Liederman, S. Jacob, Ind. Eng. Chem. Prod. Res. Dev. 12 (1973) 294.